Anisotropic Electron Spin Resonance Spectrum of PF_2 in Low-Temperature Matrices

MICHAEL S. WEI AND JERRY H. CURRENT

Department of Chemistry, University of Michigan, Ann Arbor, Michigan 48104

AND

JULIEN GENDELL

Department of Chemistry, Oakland University, Rochester, Michigan

(Received 11 August 1969)

The anisotropic electron spin resonance spectrum of the PF_2 radical has been observed. P_2F_4 was thermally decomposed by passing the gas over a hot wire. The radicals produced were trapped in an argon matrix on a flat sapphire rod held at 20°K. The same radicals were formed by photolysis of PF_2H in an argon matrix. In contrast to N_2F_4, PF_2 radicals were not detected unless the P_2F_4 was heated above 200°C. The observed 12-line ESR spectrum is interpreted as being due to randomly oriented nonrotating radicals with axially symmetric g and hyperfine tensors. Based on computer-simulated spectra, the following assignment has been made: $g_{||}=2.0011$, $g_{\perp}=1.9922$; $C_{||}(P)=307$ G, $C_{\perp}(P)=-83.0$ G; $C_{||}(F)=127$ G, $C_{\perp}(F)=33.5$ G. The same radical was also trapped in different matrices. The nature of the trapping sites and the effect of environment on the radicals is discussed. Comparison with data available for NF_2 indicates that the unpaired electron in PF_2 is localized on the central atom to a greater extent than it is in NF_2. Extended Hückel calculations also give this result.

I. INTRODUCTION

The isotropic ESR spectra of PF_2, formed by γ irradiation of ND_4PF_6 [1] and by β irradiation of PF_3 in SF_6,[2] have been reported. However, the anisotropic spectrum of PF_2 which is essential to determine the s and p character of the unpaired electron and the spin density on the individual atoms has not been reported.

This work was undertaken to investigate the conditions under which PF_2 may be generated from P_2F_4, to determine the anisotropic electron spin resonance spectrum of this radical, and to compare these data with those for NF_2.

The dissociation of P_2F_4 into 2 PF_2 radicals and the equilibrium found in the N_2F_4–NF_2 [3,4] system are significantly different.[5] It was believed by several authors[6,7] from chemical evidence that PF_2 might exist in equilibrium with P_2F_4, but no ESR spectra attributable to PF_2 were found in carbon tetrachloride[8] solutions of P_2F_4 at room temperature. Recently, Timms and Solan have identified PF_2 from heated samples of P_2F_4 using mass spectrometry.[9]

[1] J. K. S. Wan, J. R. Morton, and H. J. Bernstein, Can. J. Chem. **44**, 1957 (1966).
[2] R. W. Fessenden and R. H. Schuler, J. Chem. Phys. **45**, 1845 (1966).
[3] R. Ettinger and C. B. Colburn, Inorg. Chem. **2**, 1311 (1963).
[4] H. E. Dodrenbos and B. R. Loy, J. Chem. Phys. **39**, 293 (1963).
[5] M. Lustig, J. K. Ruff, and C. B. Colburn, J. Am. Chem. Soc. **88**, 3875 (1966).
[6] K. W. Morse and R. W. Parry, J. Am. Chem. Soc. **89**, 172 (1967).
[7] R. W. Rudolph, R. C. Taylor, and R. W. Parry, J. Am. Chem. Soc. **88**, 3729 (1966).
[8] R. W. Rudolph, Ph.D. thesis, University of Michigan, Ann Arbor, Mich., 1966.
[9] D. Solan and P. L. Timms, Chem. Commun. **1968**, 1541.

II. EXPERIMENTAL

A. Techniques

An Air-products and Chemicals, Incorporated, Cryo-Tip Model AC-2-110 was modified so that it may be used with a standard ESR cavity. This apparatus enables one to reach a temperature as low as 20.4°K (liquid-hydrogen temperature). The main features of the cold temperature cell are shown on Fig. 1. A copper rod (A) is threaded into the heat exchanger unit (B), using an indium gasket to ensure thermal contact. To the other end of the rod, which extended down into the ESR cavity, a 1-in.$\times\frac{3}{16}$-in. flat sapphire window (C) is clamped to the copper rod using a brass screw and a copper washer. A small amount of silicone grease is used to improve the thermal contact. The Cryo-Tip (D) is fitted to a brass cylinder (E) by means of vacuum O-rings; this allows rotation of the sample. The gas deposition chamber (F) is large enough to allow electric feed throughs and a $\frac{1}{4}$-in. Swagelok fitting (not shown) for the gas spray-on line on the front face. The deposition chamber may be disassembled for cleaning and altering the electrical connections by removing the top which is held on with screws (G) and an indium gasket. A piece of 11-mm quartz tubing is sealed to the bottom of (F) with an external Apiezon W seal. The quartz tubing remains in the ESR cavity during an experiment.

A metal bellows (N), which is 2.5-in. long compressed, is soldered between (E) and (F) and allows the window (C) to be raised into the deposition chamber or lowered into the quartz tube so that spectra may be taken. Two sliding cylinders (O) which are threaded to (E) and (F) guide the moving parts so that the window will not make thermal contact with the warm cell walls.

A rack soldered onto (E) and a pinion mounted on the positioning ring (P) assist in raising the window into the deposition chamber.

The whole cell may be attached to the ESR cavity by means of a counterthreaded ring. It is held firmly in place by positioning screws which are pressed against the magnet. The system is evacuated through the side-arm (Q). Temperature measurements were made using a Chromel–Constantan thermocouple (not shown in diagram) soldered to the copper rod (A).

It is possible to specifically heat a premixed sample of reactant and matrix gas by means of a small coil of 0.006-in. tungsten wire inside the gas deposition chamber (F). The wire is placed into the gas spray-on stream and spotwelded onto the two electrical feed-throughs. A small ac voltage is applied to the wire and the temperature is varied by means of a variac and a filament transformer. The approximate temperature of the hot wire is measured by means of a simple Wheatstone bridge circuit, which gives the resistance of the heated wire. The temperature then can be estimated from the temperature dependence of the resistivity of the wire. One of the advantages of this experimental setup is that the heat source, i.e., the hot tungsten wire, is close to the cold sapphire window ($\frac{3}{4}$ in. away in most experiments). Since the pressure in the deposition chamber is low (10^{-5} torr) and most of the residual gas is the matrix material, radical recombination and radical–molecule reactions are improbable.

A General Electric H4 Mercury lamp was used for the photolysis experiments. The glass face of the flood lamp was removed and no filters or focusing lenses were used. The lamp was placed one foot from the sample and photolysis was conducted in the ESR cavity, through a 50% transmitting metal grid and the quartz tube.

All the spectra were taken with a Varian 4502 spectrometer using a 100-kc/sec field modulation. A Varian magnet with 12-in.-diam pole cap and a $1\frac{3}{4}$-in. air gap was used. The X-band frequency of the microwave was measured by a TS-148/UP spectrum analyzer.

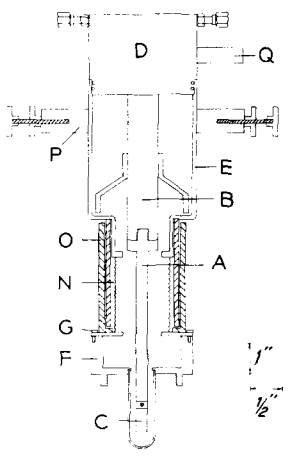

FIG. 1. Cross section of the cold cell.

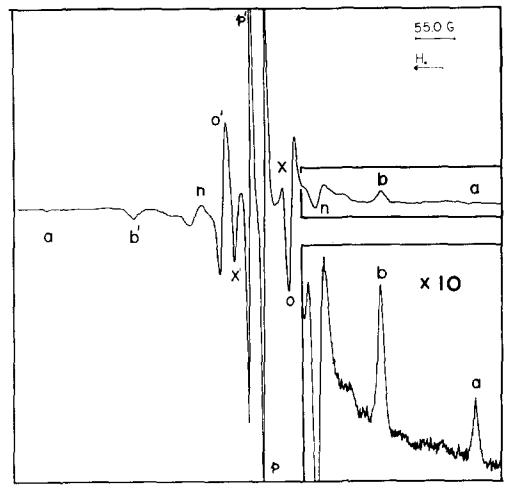

FIG. 2. Experimental ESR spectrum of PF_2, formed by the thermal decomposition of P_2F_4 in an argon matrix. The experimental sweep is ~5% nonlinear. Each measured spectrum was calibrated with the proton NMR probe.

The magnetic field was calibrated by a proton NMR probe.[10]

Ultrahigh-purity argon and research-grade krypton, xenon, and carbon dioxide were obtained from Mathison Company, Limited. Experiments were conducted with matrix gas to radical precurser molar ratios from 300:1 to 600:1. The premixed sample of reactant and matrix gas was deposited onto the cold sapphire rod through a $\frac{1}{4}$-in. stainless-steel tube. The deposition rate was controlled by a needle valve, and in most experiments, a rate of about 750 cc·cm Hg/h was used. After deposition, usually about an hour, the sample was lowered into the ESR cavity and spectra were taken. Samples of P_2F_4 and PF_2H were supplied by Hodges and Dunning of the Department of Chemistry, University of Michigan.

B. Experimental Results

Intense 12-line spectra assigned to the PF_2 radical were obtained from the thermal decomposition and the mercury lamp photolysis of both P_2F_4 and PF_2H. See Figs. 2 and 3.

In contrast to N_2F_4,[11] P_2F_4 does not dissociate at room temperature and at room-temperature spray on. However, the PF_2 radical spectrum was observed when the gaseous mixture was heated to 200°C or more.

A significant amount of PF_2 was detected at about 200°C. At about 600°C a maximum rate of formation of PF_2 was observed. This rate did not increase up to a temperature of 1200°C. Changing the M/R ratio from 300 to 600 caused no significant changes in the spectrum.

[10] B. G. Segal, M. Kaplan, and G. K. Frankel, J. Chem. Phys. **43**, 4191 (1965).

[11] J. B. Farmer, M. C. L. Gerry, and C. A. McDowell, Mol. Phys. **8**, 253 (1964).

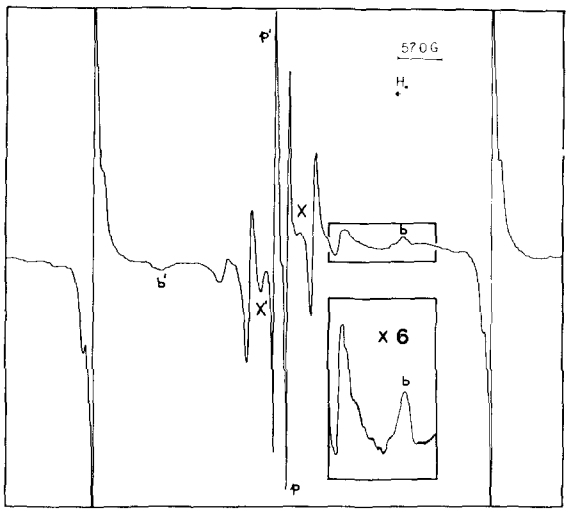

FIG. 3. Experimental ESR spectrum of PF_2 formed by the mercury lamp photolysis of PF_2H after deposition in an argon matrix.

Thermal decomposition of PF_2H was less efficient than that of P_2F_4, and a low concentration of PF_2 was observed only when the temperature of the wire was above 1000°C. No new features which might indicate PFH were observed in the spectrum. Thus fluorine atom rupture is not a competing reaction in the thermal decomposition. An attempt to obtain PF_2 by thermal decomposition of PF_3 was unsuccessful.

The photolysis of P_2F_4 and PF_2H also seems to be fairly specific in that only spectral lines assigned to PF_2 (and hydrogen atoms from PF_2H) are observed by electron spin resonance. The intensity of PF_2 signals from P_2F_4 is much less than those observed from the photolysis of PF_2H. Photolysis of P_2F_4 in a matrix is apparently much less efficient than that of PF_2H, as would be expected from the cage effect and the possibility of alternate products from P_2F_4. Photolysis of PF_2H yields a fairly high radical concentration, comparable to that obtained by thermal decomposition of P_2F_4. Hydrogen atoms are also observed as products.

The thermal decomposition products of P_2F_4 were studied in krypton, xenon, and carbon dioxide matrices. The heavy rare gases cause a broadening of the spectral lines with very little change in line positions. When CO_2 was used, the observed spectrum was very complex. The outer parallel lines were split into doublets, possibly due to different trapping sites.

The spectrum was observed while each of these samples were warmed to the point that the radical signals disappeared. In no case were signals observed which would correspond to the onset of free rotation of the PF_2 radicals. Upon warmup the PF_2 signals broadened and slowly decreased in intensity until they finally disappeared in the argon, krypton, and carbon dioxide matrices.

P_2F_4 is also known to thermally decompose into PF_3 and the PF radical which may be trapped in a matrix.[12] The PF radical is in a $^3\Sigma$ ground state.[13] The ESR spectrum of O_2, which is similar to PF, has not been observed when O_2 is trapped in inert matrices; and one would therefore not expect to detect PF under these conditions.

III. SIMPLE MO DESCRIPTION OF PF_2

PF_2, a 19-electron radical, is expected to have a C_{2v} symmetry with the molecular axes defined as shown in Fig. 4. The angle is expected to be approximately equal to that of NF_2, which is 104°.[14] The expected electronic configuration is $(1a_1)^2(1b_2)^2(2a_1)^2(1b_1)^2(3a_1)^2(4a_1)^2(2b_2)^2(1a_2)^2(3b_2)^2(2b_1)^1$, with a $^2B_1$ ground state[15]

$$\psi_{\mathrm{mo}}(2b_1) = \alpha_1 P(p_x) - \{\alpha_2/\sqrt{2}[F(p_{x1}) + F(p_{x2})]\} \quad (1)$$

with

$$|\alpha_1|^2 + |\alpha_2|^2 \simeq 1,$$

where $F(p_{x1})$ indicates the p_x orbital on fluorine atom one, etc.

Since the unpaired electron is expected to be a linear combination of phosphorus and fluorine p_x orbitals, the x axis should show the largest anisotropic hyperfine splittings and it is designated as the parallel magnetic axis. The dipolar part of hyperfine splittings in the y and z directions is expected to be on the order of $\frac{1}{2}$ of that found for the x axis.[16]

IV. ANALYSIS OF SPECTRA

The spectra shown in Figs. 2 and 3 are believed to be due to PF_2 radicals. That identical spectra were produced using different methods (thermal decomposition and photolysis), and different radical precursors (P_2F_4 and PF_2H), is a strong indication that the trapped species is PF_2. The two outermost lines in Fig. 3 are due to hydrogen atoms, the g value of which is found to be 2.0011 and the hyperfine splitting is 509.5 G. The a and a' lines are apparently obscured by the hydrogen atom lines.

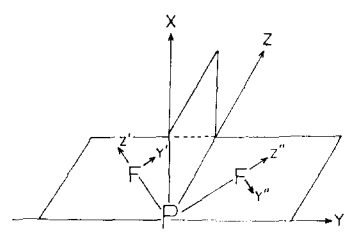

FIG. 4. Molecular and atomic axes for PF_2.

[12] D. Solan, University of California, Berkeley, Calif. (personal communication, 1969).
[13] A. E. Douglas and M. Frąckowiak, Can. J. Phys. **40**, 832 (1962).
[14] M. D. Harmony, R. J. Myers, L. J. Schoen, D. R. Lide, and D. E. Mann, J. Chem. Phys. **35**, 1129 (1961).
[15] A. D. Walsh, J. Chem. Soc. **1953**, 2266.
[16] A. Carrington and A. D. McLachlan, *Introduction to Magnetic Resonance* (Harper and Row Publishers, Inc., New York, 1967), p. 110.

The spectra indicate that PF_2 has axially symmetric hyperfine and g tensors, with the parallel component presumably along the molecular x axis which is perpendicular to the molecular plane. The y and z axes are apparently magnetically equivalent. The lines marked as a, a', b, b', and x, x' in the spectra are designated as the parallel components, whereas p and p' and the remaining four lines are the perpendicular components. The basis for this assignment is discussed later.

A. Orientation Effects

A preferential orientation of radicals in a sample is an aid in the assignment of the principal axes of the hyperfine tensors. A change in the relative intensities of the parallel and perpendicular lines will be observed on rotating the sample with respect to the static field. The largest intensity change should occur in the parallel lines. A small amount of preferential orientation is observed in our spectra. Kasai, Weltner, and Whipple have reported the preferential orientation of NO_2 [17] and $Cu(NO_3)_2$ [18] in neon matrices. These radicals have a high tendency to align themselves with their molecular plane parallel to the surface of the matrix on the flat sapphire window. They[17,18] also reported that preferential orientation is most pronounced when neon is used as a matrix. It is not possible to use neon as a matrix with this experimental arrangement since liquid hydrogen is used as the refrigeration source.

Using argon matrices, small changes in the spectrum were observed upon rotation of the sapphire window from the spray-on position parallel to the magnetic field to an orientation perpendicular to the magnetic field. Lines a, a' and b, b' increased by a factor of 2; x and x' also showed a change in intensity. The two most intense peaks, p and p' showed a small change in line shape, whereas the remaining four lines remained vitrually unchanged. These are strong indications that the radicals are preferentially deposited with their molecular plane parallel to the surface of the forming matrix, and that lines a, a', b, b', and x, x' correspond to orientations with the static magnetic field perpendicular to the molecular plane. Thus, these lines are designated as the $\|$ features. The remaining six lines are then the $\perp$ features, with the phosphorus splitting greater than twice the fluorine splitting, giving two pairs of triplets. It should be noted that the triplets do not have the 1:2:1 intensity distribution expected for the isotropic spectra of two equivalent spin-$\frac{1}{2}$ nuclei. However, this is typical of an amorphous sample in which each orientation of the radical with respect to the static field gives a different contribution to the spectrum. This assignment of $\|$ and $\perp$ features, attributing the larger hyperfine splittings to the $\|$ orientation, is in agreement with expectations based on the simple MO description found in Sec. III.

B. First-Order Calculation

Computer spectrum simulation programs were written to aid in the analysis of the spectra. The computer was programmed to calculate the field values, correct to first order for a given orientation of the radical with respect to the field. For axial cases 90 values of θ were used and a "stick spectrum" generated. Transition probabilities were assumed to be field independent since the $g_{\|}$ and $g_{\perp}$ values are observed to be very nearly equal.

A Gaussian derivative line shape with a constant line width and intensity proportional to the intensity of the "stick spectrum" was generated at each of the 2000 "stick spectrum" locations. The sum of these Gaussian derivarive contributions was plotted using a Calcomp plotter. Calculations were done on an IBM 360/67 computer. The line width corresponds to $(1/T_2)$ in the standard formulation or one half of the peak-to-peak distance in a Gaussian derivative curve. The nuclear Zeeman and "first-order" forbidden transitions are calculated[19] to have a negligible effect on the spectrum, and they are not included in the program.

Comparison of this first-order computed spectrum with the experimental spectra indicates reasonable agreement with general features and the line positions. Prior to making the appropriate second-order corrections, the apparent values of $g_{\|}$ and $g_{\perp}$ are 2.0020 and 2.0025, respectively.

C. Second-Order Calculation

The spectrum was also simultated including the second-order splittings, for axially symmetric hyperfine tensors and two equivalent fluorine nuclei.

Maruani *et al.*[20] have given an approximate formula for the second-order corrections in the case of several spin-$\frac{1}{2}$ nuclei with possibly different principal directions of hyperfine tensors. Their approximation is not valid, however, for the case of equivalent nuclei (or more precisely, when the difference between the hyperfine coupling of the two nuclei is the order of, or less than, the second-order correction), which must be considered for axially symmetric PF_2. In particular, for the two equivalent nuclei, the two states which are degenerate to first order are split when the second-order effect is included.

In the case of PF_2, if the fluorine hyperfine tensors have axial symmetry, then the two fluorine nuclei are magnetically equivalent for all orientations of the static magnetic field. We have calculated the second-order correction for this case in the following manner. The g tensor was assumed to be isotropic, (since $g_{\|}-g_{\perp}\simeq$

[17] P. H. Kasai, W. Weltner, Jr., and E. B. Whipple, J. Chem. Phys. **42**, 1120 (1965).
[18] P. H. Kasai, E. B. Whipple, and W. Weltner, Jr., J. Chem. Phys., **44**, 2581 (1966).
[19] R. Lefebvre and J. Maruani, J. Chem. Phys. **42**, 1480 (1965)
[20] J. Maruani, C. A. McDowell, H. Nakajima, and P. Raghunathan, Mol. Phys. **14**, 349 (1968).

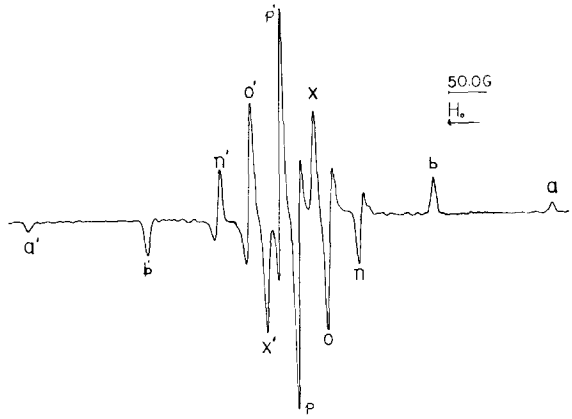

FIG. 5. Second-order computer simulated spectrum of a randomly oriented sample of PF_2 using a Gaussian derivative shape with a constant linewidth of 2.5 G. The linewidth is defined as half the peak to peak separation of the derivative of a Gaussian distribution. The parameters are the experimental values for argon matrices found in Table IV.

0.009) and the hyperfine tensor were assumed to have axial symmetry with principal values $C_{||}$ and $C_\perp$. The Hamiltonian was expressed in the axis system with the z axis along the direction of the static field H_0. The energies and eigenvectors were obtained explicitly to first order (i.e., using the first-order Hamiltonian):

$$\mathcal{H}_1=(g\beta/H_0)\,S_z+(C_\perp\sin^2\theta+C_{||}\cos^2\theta)\,S_zI_z + (C_{||}-C_\perp)\cos\theta\sin\theta S_zI_y, \quad (2)$$

where θ is the angle between H_0 and $C_{||}$. Employing these energies and eigenvectors, the second-order corrections were calculated by perturbation theory using the remaining part of the Hamiltonian,

$$\mathcal{H}_2=C_\perp S_xI_x+(C_\perp\cos^2\theta-C_{||}\sin^2\theta)\,S_yI_y + (C_{||}-C_\perp)\cos\theta\sin\theta S_yI_z. \quad (3)$$

The inclusion of second-order effects shifted the $\perp$ spectral features more than the $||$ features. Thus $g_{||}$ is in fact 0.0089 greater than $g_\perp$ rather than the 0.0005 difference obtained from the direct measurement of the spectrum. The computer simulation spectrum is shown in Fig. 5.

The second-order calculation split the "stick spectrum" contribution of the "degenerate" lines. It was expected that this would be observed in the final calculated derivative spectrum since the splitting is 14 G for the components when the $||$ axis is perpendicular to the magnetic field. However, no splitting of the degenerate lines is observed nor are these lines shifted with respect to the other $\perp$ features. Their intensities are reduced somewhat by inclusion of the second-order splittings. The low-field components from the degenerate lines apparently do not accumulate sufficiently at any field value ("stick spectrum" location) to be observable in the derivative spectrum.

With the exception of the relative change in g components, the inclusion of second-order effects caused only small changes in the computer simulated spectrum. We have therefore used the less expensive first-order program to test other variables in the calculation.

D. Results

Based on computer simulation including the second-order effects, the diagonal elements of the g tensor for PF_2 in an argon matrix are determined to be

$$g_{||}=g_{xx}=2.0011\pm0.0005,$$
$$g_\perp=g_{yy}=g_{zz}=1.9922\pm0.0005.$$

The observed hyperfine splittings are[21]

P: $C_{||}=C_{xx}=307\pm2$ G,
$C_\perp=C_{yy}=C_{zz}=-83.0\pm0.5$ G;

F: $C_{||}=C_{xx}=127\pm2$ G,
$C_\perp=C_{yy}=C_{zz}=33.5\pm0.5$ G.

E. Linewidth Effects

There is excellent agreement between the line positions of the experimental and computed spectra and generally good agreement of line intensities. There is, however, a noticeable disagreement between the calcalculated and experimental spectrum in that the ratio of the parallel-to-perpendicular line intensities appears to be larger in the computed spectra. A plausible explanation for this discrepancy is that experimentally the linewidths of the parallel features are observed to be broader than those of the perpendicular ones; yet, a constant linewidth was used for the computed spectra. A major source of line broadening is a distribution of hyperfine parameters due to slight differences between sites for the PF_2 radical in the matrix. Such changes in hyperfine splittings for PF_2 have been observed when CO_2 or krypton was used as a host matrix. See Sec. V.D. The parallel components, having larger hyperfine splittings, will probably have a larger spread of line positions than the perpendicular components due to a variation in the radical sites. Without detailed knowledge of the radical–matrix interaction, one does not know how the linewidth varies with orientation. To take into account in an approximate manner this angular linewidth dependence, we arbitrarily assumed that the linewidth has the same functional dependence on orientation as

[21] The choice of the signs for the components of the hyperfine tensors is based on two factors. The first is that the parallel dipolar parts of the tensor ($B_{||}$) should be positive, and the second is that the isotropic part of the hyperfine tensor should be approximately equal to the isotropic values reported by Wan and Morton. (See Sec. V.B.) These assignments result in positive signs for the isotropic parts of the hyperfine tensors.

the g and hyperfine tensors.[22] Specifically we computed a spectrum with the linewidth λ, varying with the angle θ as $\lambda(\theta)=(\lambda_\perp^2\sin^2\theta+\lambda_{||}^2\cos^2\theta)^{1/2}$. Using $\lambda_\perp=2.5$ G and $\lambda_{||}=6.0$ G, much better agreement was obtained (Fig. 6).

Closer examination of the experimental spectra indicates that all the perpendicular components do not have the same width; the outer lines (n and n' in Fig. 2) are distinctly broader than the inner ones. This is consistent with the model for line broadening based on varying matrix site interactions. Consider two sites causing a difference in hyperfine parameters ΔC_P and ΔC_F, for a given orientation. The ESR spectrum would consist of six component lines labelled by the six combinations of m_P and m_F, (the quantum numbers for the phosphorus and fluorine nuclei, respectively). The difference in line position for each of these six components is given by $\Delta H=m_P\Delta C_P+m_F\Delta C_F$. It is therefor evident that ΔH is not constant but is different for the different component lines. If we consider a distribution of values for ΔC_P and ΔC_F, corresponding to a distribution of radical sites in the matrix, and realize that ΔC_P and ΔC_F are not independent variables but are related to one another, then different apparent linewidths for the six components would result. The outermost $\perp$ components (n and n' in Fig. 2) have $m_P=+\frac{1}{2}$, $m_F=-1$, and $m_P=-\frac{1}{2}$, $m_F=1$ [since $C_\perp(P)$ is negative and $C_\perp(F)$ is positive]. And thus, if ΔC_P and ΔC_F are of opposite sign, the outermost $\perp$ components (n and n' in Fig. 2) would be broader than the inner ones (o, p and o', p' in Fig. 2) as is observed experimentally. Similar considerations apply to the $||$ components but here the innermost $||$ components (x and x') are most broadened.

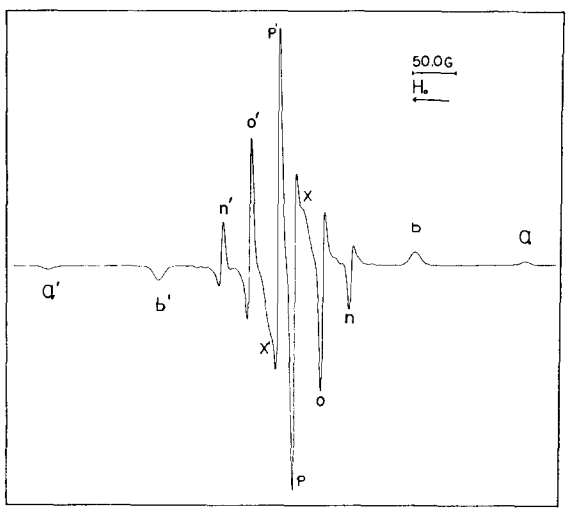

FIG. 6. Computer simulated first derivative spectrum of a randomly oriented sample of PF_2 using the Gaussian line shape with variable linewidth. $\lambda_{||}=6.0$ G; $\lambda_\perp=2.5$ G.

[22] The shape of a calculated derivative spectrum is apparently most sensitive to the choice of parameters in the vicinity of the canonical orientations. The values of $\lambda_{||}$ and $\lambda_\perp$ are of prime importance, and the way in which the width varies with orientation is much less significant.

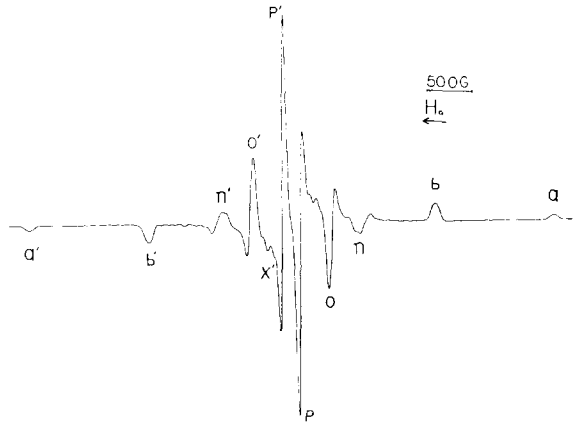

FIG. 7. Computer simulated spectrum of PF_2 made by summing five spectra with equal intensity (i, ii, iii, iv, v) having correlated variations of phosphorus and fluorine hyperfine tensors. The changes in the diagonal hyperfine values (in Gauss) for each of the five spectra from those found in Table IV are: (i) $\Delta C_\perp(F)=3.0$, $\Delta C_{||}(F)=9.0$, $\Delta C_\perp(P)=-6.0$, $\Delta C_{||}(P)=-9.0$; (ii) $\Delta C_\perp(F)=1.5$, $\Delta C_{||}(F)=4.5$, $\Delta C_\perp(P)=-3.0$, $\Delta C_{||}(P)=-4.5$; (iii) $\Delta C_\perp(F)=0.0$, $\Delta C_{||}(F)=0.0$, $\Delta C_\perp(P)=0.0$, $\Delta C_{||}(P)=0.0$; (iv) $\Delta C_\perp(F)=-1.5$, $\Delta C_{||}(F)=-4.5$, $\Delta C_\perp(P)=3.0$, $\Delta C_{||}(P)=4.5$; (v) $\Delta C_\perp(F)=-3.0$; $\Delta C_{||}(F)=-9.0$, $\Delta C_\perp(P)=6.0$, $\Delta C_{||}(P)=9.0$. A constant Gaussian linewidth of 2.5 G was used.

An approximate inclusion of this linewidth effect in the calculation of the spectrum results in better agreement between the line intensities of the experimental and computed spectra. See Fig. 7.

On the basis of the good agreement between the experimental and computed spectra and the fact that instances of line-intensity disagreement can be accounted for, we feel that our analysis of the spectrum and the values for the magnetic parameters are essentially correct. However, a number of alternate possibilities have been tested and the results of these calculations are described in the next section.

F. Nonaxial Model Calculations

For systems of three spin-$\frac{1}{2}$ nuclei, two of which are equivalent, a 12-line pattern is a strong indication that the hyperfine tensors have axial symmetry. A rhombic pattern would yield 18 lines. However it is possible that the lines are sufficiently overlapped so that the total number of observable lines is reduced. We have tested the following possibilities, with axial and rhombic g tensors:

(1) nonaxial hfs of P, axial hfs of F;
(2) nonaxial hfs of P, nonaxial hfs of F;
(3) nonaxial hfs of P, nonaxial hfs of F, principal axes of P and F hfs nonequivalent;
(4) axial hfs of P, nonaxial hfs of F, principal axes of P and F nonequivalent.

All these plausible interpretations were tested with the

computer program. Poor agreements were obtained in the first three cases, whereas the investigation of No. (4) produced some interesting insights as to the nature of the P–F bond. More detail is discussed in the following section.

G. The Magnetic Axes

One of the principal axes of the g tensor and the hyperfine tensors of each nucleus should certainly be parallel to the x molecular axis, since the various p_x atomic orbitals are the primary components of the unpaired electron MO [Eq. (1)]. Another axis of the g tensor and the phosphorus hyperfine tensor coincides with the z axis (the C_2 axis) of the molecule. Thus the third axis for these two tensors is defined by the y molecular axis.

Since the magnetic axes of the phosphorus atom are parallel to the g axes, no off-diagonal terms are possible in the phosphorus hyperfine tensor. Any nonaxial nature in this diagonal tensor would be seen as a simple splitting in the six-line $\perp$ spectrum. Since these are not observed, the phosphorus hyperfine tensor is thus believed to be axial.

The fluorine atoms are, however, not so easily considered since the fluorine hyperfine tensors may have their principal directions along and perpendicular to the P–F bonds, i.e., along x, y', z' and x, y'', z'' (Fig. 4). Thus, transformation of the hyperfine tensors to coincide with the g-tensor principal axes will result in off-diagonal elements, which may produce unpredictable line positions and line shapes. This situation has been explored by Maruani *et al.* for CF_3 radicals in argon matrices.[20]

The effect of nonaxial fluorine hyperfine tensors having one principal axis along the P–F bond has been studied by computer simulated spectra, using only the first-order approximation.

Fluorine hyperfine tensors with their principal axes along and perpendicular to the P–F bonds were used having diagonal values of 307, 31, and 36 G. Transforming these tensors to the molecular axis system yields off-diagonal values for each of the fluorine nuclei; $(C_{yz})_1 = (C_{zy})_1 = 2.5$ G; and $(C_{yz})_2 = (C_{zy})_2 = -2.5$ G. The computer simulated spectrum is identical to those calculated with axially symmetric fluorine hyperfine tensors. If however $|C_{y'y'} - C_{z'z'}| > 6$ G, splitting of the degenerate lines is observed. The fluorine hyperfine tensors are thus believed to be axial, or nearly axial, with a small amount of nonaxial character being undetectable for the observed experimental linewidth.

Based on theoretical models, the y' and z' hyperfine components are expected to be nearly equal since the only fluorine contribution to the half-filled molecular orbital is p_x. Polarization of the P–F bond may cause the tensors to become nonaxial. However, this type of interaction is expected to be quite small[23] and the dipolar hyperfine coupling tensors should be axial, with at most a 10% or 15% deviation from axial symmetry.

V. DISCUSSION

A. Rotation in the Matrix

An apparent axial symmetry would result if the radicals were specifically rotating in the molecular plane even if the hyperfine tensors were nonaxial. Complete free rotation in the matrix is not found for the radical since $\parallel$ and $\perp$ components and partial preferential orientation of the radicals are observed. Furthermore, free rotation could not be induced by increasing the size of the matrix atoms or by elevating the temperature to the diffusion temperatures of the individual matrices used. That is, the parallel and perpendicular components were still observed at the highest possible temperatures.

It seems doubtful that the x axis is sufficiently unique that rotation would occur about it under these various experimental conditions, yet it could still be held fixed in the matrix. We conclude that the PF_2 radical is not rotating in the matrix about any axis and that the hyperfine tensors must be axial or nearly axial. The NF_2 radical has also been found to be not rotating in rare-gas matrices.[24]

B. g Value

The g values deviate somewhat from the free electron value ($g_e = 2.0023$). The mixing of electronic states can change the g value, via the spin–orbit coupling interaction. For an atomic system, this can be represented as $\xi \mathbf{L}\cdot\mathbf{S}$, where ξ is the spin–orbit coupling constant.

However, the spin–orbit coupling operator for an electron in a molecule no longer assumes such simple form, because the electron moves over several atoms, each having a different value of ξ. The full spin–orbit Hamiltonian can be written approximately as

$$\mathcal{H}_{LS} = \sum_k \xi_k(\mathbf{r}_k)\mathbf{L}_k\cdot\mathbf{S}$$

where

$$\xi_k(\mathbf{r}_k) = (e\hbar^2/2m^2c^4)\{\mathbf{r}_k^{-1}[\partial V(\mathbf{r}_k)/\partial \mathbf{r}_k]\}$$

and $\mathbf{L}_k$ is the orbital angular momentum about the center of the kth atom.

Using such an expression to calculate the g value would be very difficult. However, it is possible to adopt a simpler expression if certain approximations are made[25,26]:

(1) Since $\xi_k(\mathbf{r}_k)$ decreases rapidly with increasing $\mathbf{r}_k$ [$\xi_k(\mathbf{r}_k) \sim r^{-3}$ for large r], it can be treated effectively as

[23] A. Hinchliffe and J. N. Murrell, Mol. Phys. **14**, 147 (1968).

[24] P. H. Kasai and E. B. Whipple, Mol. Phys. **9**, 497 (1965).

[25] A. J. Stone, Proc. Roy. Soc. (London) **271A**, 424 (1963).

[26] H. C. Longuet-Higgins and A. J. Stone, Mol. Phys. **5**, 417 (1962).

zero except near atom k; thus it can be replaced by ζ_k (the appropriate spin–orbit function for the kth atom).

(2) The electrons move in an independent set of molecular orbitals. All but one of the occupied orbitals contain two electrons and it is the unpaired electron alone that contributes to the g tensor.

Based on these assumptions, a much simplified expression is obtained:

$$g_{xx} \simeq g_e + 2\sum_n{}' \sum_{k,j} \frac{\langle \psi_0 \mid \zeta_k L_{xk} \delta_k \mid \psi_n \rangle \langle \psi_n \mid L_{xj} \delta_j \mid \psi_0 \rangle}{E_0 - E_n}, \quad (4)$$

where ζ_k is the spin–orbit coupling of the kth atom, in our case, ζ_P, ζ_F; ψ_0 is the ground-state wavefunction; ψ_n is the occupied or unoccupied molecular orbitals. Two other similar expressions can be written for g_{yy} and g_{zz}. For a molecule like PF_2 with C_{2v} symmetry, the L_x, L_y, and L_z components of the orbital angular momentum transform according to B_2, B_1, and A_2, respectively. Since ψ_0 is of the symmetry class B_1, the nonzero terms in Eq. (4) require ψ_n to be of class A_2 ($\langle B_1 \mid L_x \mid A_2 \rangle$). Contributing terms in g_{yy} are of the form $\langle B_1 \mid L_y \mid A_1 \rangle$ and contributing terms in g_{zz} are of the form $\langle B_1 \mid L_z \mid B_2 \rangle$.

The coefficients for the atomic orbitals, and orbital energies can be estimated by LCAO molecular-orbital calculations and the nonzero terms in Eq. (4) can be evaluated.

1. Hückel MO Calculations

Extended Hückel MO calculations were made on the PF_2 systems both with and without d-orbital contributions. Similar calculations were also performed for NF_2. The computer program which was used is a version of Hoffmann's[27] program which has been modified by Su, Department of Chemistry, University of Michigan, to include d-orbital contributions. The program calculates the coefficients of the atomic orbitals and the molecular-orbital energies. The squares of the coefficients for the half-filled orbital define the calculated spin densities on the atoms. The calculations show only a slight dependence of these coefficients on the bond angle. Thus no bond-angle information can be expected for PF_2 from a comparison of the results of the ESR experiments and these calculations.

The atomic orbital ionization potentials used are given in Table I. The constant "K" (the proportionality constant between the resonance integral for two atoms and the product of the overlap integral and the mean of the Coulomb integrals) was set at 2.00 for most calculations. The P–F bond length was set at 1.58 Å as found in PF_2H.[28] Since the calculations are insensitive to the bond angle, an angle of 102° was arbitrarily used for PF_2. The N–F bond distance of 1.40 Å[29] and an angle of 104° were used in the NF_2 calculations.:

TABLE I. Atomic-orbital ionization potentials used in the Hückel calculations (electron volts).

Atom	P	F	N
$2s$		−42.51	−28.13
$2p$		−17.42	−14.54
$3s$	−20.30		
$3p$	−11.00		
$3d$	−2.50		

Some results of the calculations are:

(a) The unpaired electron for both PF_2 and NF_2 goes into an orbital of $2b_1$ symmetry, composed primarily of p_x orbitals on phosphorus and fluorine as expected. For PF_2 the amount of d-orbital contribution to the B_1 orbital is very small.

(b) For PF_2 the MO's above the half-filled $2b_1$ orbital have the order (in increasing energy from $2b_1$) $(4b_2) \simeq (5a_1)$; $(3b_1) \simeq (2a_2) \simeq (6a_1)$; $(7a_1)$; $(5b_2)$.

(c) The lowest two unfilled orbitals in PF_2 are much closer to the half-filled $(2b_1)$ orbitals when d orbitals are included.

(d) Calculations on NF_2 indicate a generally smaller spread in the filled orbital energies than found for PF_2. However, since d orbitals are not included, there is a relatively large gap to the first empty orbital.

(e) For $1.25 < K < 2.1$, the $(1b_1)$, $(3a_1)$, $(4a_1)$, $(2b_2)$, $(1a_2)$, and $(3b_2)$ orbitals appear much more closely spaced than the typical Walsh diagram[15] would lead one to believe. They were within 1 eV in all calculations.

2. g_{xx}

There is one filled orbital and one empty orbital of symmetry class A_2. In addition, if d orbitals are not included all matrix elements of L_x are zero and there would be no change in g_{xx}. Inclusion of the d orbitals results in some g_{xx} shift. For PF_2, a change in g_{xx} of 0.0001 smaller than the free-electron value is calculated. This is in fair agreement with our experimental value, ($g_{xx} = 2.0011$).

3. g_{yy} and g_{zz}

Our experiments indicate an axial g tensor for PF_2, i.e., $g_{yy} = g_{zz} = g_\perp$, with $g_\perp$ less than the free-electron value. There are four filled and three unfilled orbitals of the class A_1. Using the orbital coefficients and energies from the extended Hückel treatment, a positive shift in g_{yy} is calculated. As for the z component, there are three filled and two unfilled orbitals of symmetry class B_2. A similar calculation showed that g_{zz} is smaller than the free electron value and is also smaller than the experimentally observed quantity. It is apparent that these

[27] R. Hoffmann, J. Chem. Phys. **39**, 1397 (1963).
[28] R. L. Kuczkowski, J. Am. Chem. Soc. **90**, 1905 (1968).
[29] D. R. Lide, Jr., J. Chem. Phys. **38**, 456 (1963).

TABLE II. Comparison of experimental and calculated g values.

	NF_2		PF_2	
	Calculated	Experimental[a]	Calculated	Experimental
g_{xx}	2.0023	2.0011±0.0005	2.0022	2.0011±0.0005
g_{yy}	2.0099	2.0079±0.0005	2.0075	1.9922±0.0005
g_{zz}	2.0061	2.0042±0.0005	1.9893	1.9922±0.0005

[a] See Ref. 24.

calculations overestimate the g component in one axis and underestimate it in the other axis.

Similar calculations of g values were also performed for NF_2. The results, together with the experimental values are tabulated in Table II.

B. Hyperfine Tensors

A hyperfine coupling tensor can be resolved into an isotropic part $\mathfrak{A}_c$ and a dipolar part $\mathbf{B}$ as follows: $\mathbf{C}=\mathfrak{A}_c\mathbf{U}+\mathbf{B}$, where $\mathbf{U}$ = unit tensor. For the PF_2 radical, the unpaired electron is in a π-antibonding orbital, which is a linear combination of the phosphorus $3p_x$ and fluorine $2p_x$ orbitals. The traceless dipolar hyperfine tensor for each atom should be axially symmetric with its principal values equal to $(B_x, -\frac{1}{2}B_x, -\frac{1}{2}B_x)$ if polarization of bonding orbitals is negligible. Since the electron–nuclear dipolar coupling is positive along the axis of a p orbital, B_x is taken as positive. Using this model the hyperfine tensors are resolved into their dipolar and isotropic parts:

P: $B_{||}=B_{xx}=260$ G,

$B_{\perp}=B_{yy}=B_{zz}=-130$ G,

$\mathfrak{A}_c=47$ G;

F: $B_{||}=B_{xx}=62$ G,

$B_{\perp}=B_{yy}=B_{zz}=-31$ G,

$\mathfrak{A}_c=65$ G.

These values of the isotropic splitting constants seem to be somewhat higher than those reported by Wan and Morton.[1] This is probably due to the fact that PF_2 is trapped in a different matrix environment. Their radicals were in an ionic crystal as opposed to the inert-gas matrices used in this work.[30]

It is possible to obtain an estimate of spin populations of the unpaired electron on each atom by comparing the observed value to some known reference value.[31] The spin densities on the s-type orbitals are then estimated to be

$$\mathfrak{A}_c(\mathrm{P})/\mathfrak{A}_c^{\mathrm{ref}}(\mathrm{P})\simeq 47/3640\simeq 0.013,$$

$$\mathfrak{A}_c(\mathrm{F})/\mathfrak{A}_c^{\mathrm{ref}}(\mathrm{F})\simeq 65/17\,200\simeq 0.0038.$$

PF_2 is a π radical in which no s-type orbital contributes to the unpaired electron MO and hence isotropic splitting is observed when the inner s shells are polarized by the odd electron in the p orbitals. This type of inner-shell polarization is expected to be small, as is found experimentally.

Using a similar expression, the p-type spin density on phosphorus and fluorine are estimated:

$$|\alpha_1|^2\simeq B_x(\mathrm{P})/B_x^{\mathrm{ref}}(\mathrm{P})\simeq 260/206\simeq 1.26,$$

$$\tfrac{1}{2}|\alpha_2|^2\simeq B_x(\mathrm{F})/B_x^{\mathrm{ref}}(\mathrm{F})\simeq 62/1084\simeq 0.06. \quad (5)$$

The spin density on phosphorus and fluorine do not add up to unity as expected. However, these values are not to be taken literally, due to the nature of the approximations involved in Eq. (5). The experimentally determined quantities are the result of interactions between an unpaired electron spin and the magnetic nuclei of the molecule which is trapped in a rare gas matrix. However, the reference values are calculated for isolated atoms. The relative magnitudes of $|\alpha_1|^2$ and $|\alpha_2|^2$ indicate, however, that the unpaired electron is mainly localized on the phosphorus atom.

From the coefficients of the eigenvectors in the extended Hückel calculation, the same type of spin density distribution is also observed. The results for PF_2, together with those for NF_2, are tabulated in Table III. The excellent agreement between the calculated and experimental values, normalized to one electron, is probably fortuitous, although the calculated orbital coefficients are very much less dependent on the arbitrary constant K than are the orbital energies.

TABLE III. p-orbital spin densities for PF_2 and NF_2.

	PF_2		NF_2[c]	
	P	F	N	F
Experimental[a]	1.26	0.06	1.0	0.15
Normalized experimental	0.91	0.045	0.76	0.12
Calculated[b]	0.88	0.06	0.76	0.12

[a] Experimental values were obtained by using Eq. (5).
[b] Results of the extended Hückel calculation. See text.
[c] See Ref. 24.

[30] Numerous examples of changes in the g and the hyperfine tensors with a change in matrix environment may be cited. An extensive tabulation of data for NO_2 may be found in: T. J. Schaafsma, G. A. V. D. Velde, and J. Kommandeur, Mol. Phys. **14**, 501 (1968). Other examples are tabulated by P. W. Atkins and M. C. R. Symons, *The Structure of Inorganic Radicals* (Elsevier Publ. Corp., New York, 1967).

[31] P. W. Atkins and M. C. R. Symons, *The Structure of Inorganic Radicals* (Elsevier Publ. Corp., New York, 1967), p. 21.

TABLE IV. Experimental g and hyperfine tensors for PF_2 in different matrices.

	$g_\perp$[a]	$g_\parallel$[a]	$C_{\perp F}$	$C_{\parallel F}$	$C_{\perp P}$	$C_{\parallel P}$
Argon	1.9922	2.0011	33.5±0.5	127±2	−83.0±0.5	307±2
Krypton	1.992±0.001	2.000	34±1	123±3	−86±4	307±3
Xenon	1.992±0.001	...	32±5	...	−85±3	...
CO_2(a)	1.990±0.001	2.0001	20±4	120±5	−78±4	327±5
CO_2(b)	1.992±0.001	2.0004	12±5	107±5	−36±5	342±5

[a] Including second-order correction.

C. Comparison of NF_2 and PF_2

The diagonal elements of the dipolar part of the fluorine hyperfine tensors for NF_2 are reported[24] as (152, −76, −76) in Gauss units. The diagonal fluorine components for PF_2 are (62, −31, −31). Thus, the spin density on the fluorine atoms in PF_2 is less than that on NF_2. This can be rationalized as follows: The difference in electronegativity between fluorine and the central atom must operate so as to concentrate the bonding electrons on the fluorine atoms, leaving the unapired electron localized mainly on the central atom. Since phosphorus is more electropositive than nitrogen, this effect should be more pronounced in PF_2 than in NF_2.

The same conclusion can be reached by consideration of a simple MO model. The valence orbitals of nitrogen are of comparable energy to those of fluorine since they are both in the same principal quantum shell, while the valence orbitals on phosphorus are higher in energy. Thus the interaction between the phosphorus valence orbitals and the fluorine valence orbitals will be less than the nitrogen and fluorine orbital interaction. Since for both PF_2 and NF_2, the 19th electron is in an antibonding orbital with the unpaired electron primarily localized on the central atom, less interaction between the central atom and the fluorine will put more spin density on phosphorus in PF_2 than nitrogen in NF_2. This difference in spin density on the central atom is also obtained from the results of the approximate MO calculations we have performed (see Table III).

The relatively high electron spin density on phosphorus may explain the stability of P_2F_4 with respect to dissociation as compared to N_2F_4. In PF_2 the unpaired electron is not as delocalized as it is in NF_2 so there is less of an energy term favoring radical formation.

D. Matrix Effects

PF_2 was studied in other matrices (Kr, Xe, CO_2) in an effort to obtain an isotropic spectrum of freely rotating radicals and to investigate matrix–radical interactions. In no case was an isotropic spectrum observed. In krypton and xenon matrices the spectrum of PF_2 was essentially the same as that in argon. Small splittings in the p and o lines were observed in the krypton matrix and the lines were broader in both matrices. The g values and the hyperfine splitting constants are given in Table IV. The linewidths of the parallel components increased from ~4 G in argon to ~7 G in krypton to unmeasurably broad lines in xenon. The parallel lines in the xenon matrix were barely observable above the noise level even though the center line intensities showed a large sample of PF_2 was present. The experimental linewidths were measured as $\frac{1}{2}\times$ (width at half-height) of the parallel lines. The

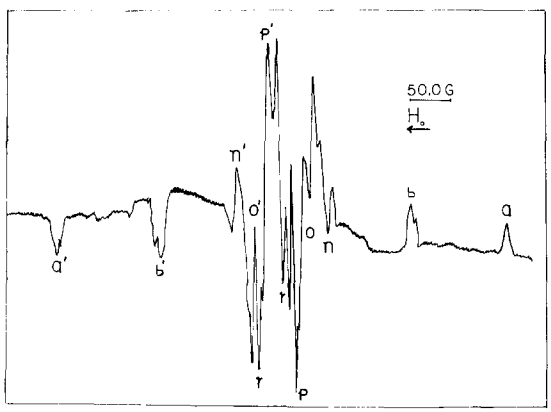

FIG. 8. Experimental ESR spectrum of PF_2 formed by thermal decomposition of P_2F_4 and deposited with a CO_2 matrix.

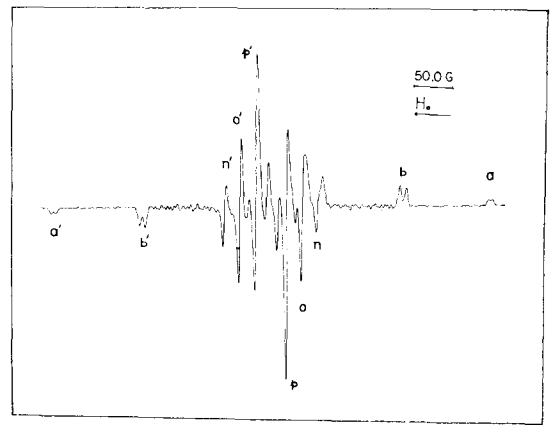

FIG. 9. Computer simulation of the first derivative spectrum of a randomly oriented sample of PF_2 using the superposition of two sets of axial hyperfine tensors. (See Table IV). The Gaussian line shape with a width of 2.0 G was used.

TABLE V. Dipolar and isotropic components of the hyperfine tensors in argon and CO_2 matrices in gauss.

	$B_{\|\|}$(P)	$B_{\|\|}$(F)	a(P)	a(F)	Phosphorous s-spin density	Fluorine s-spin density
Argon	260	62	47	65	0.013	0.0038
CO_2(a)	270	67	57	53	0.016	0.0031
CO_2(b)	252	63	90	44	0.025	0.0026

perpendicular lines are also broader in krypton and xenon. The experimental linewidths (measured as one-half the peak-to-peak distance) vary from line to line in each matrix. In argon the apparent linewidths are 5.5, 3, and 1 G for the lines n, o, and p (Fig. 2). In xenon, n is unobservably broad at 20°K. o and p are 11 and 4 G, respectively. Warming the xenon matrix to 50°K reversibily narrows the n, o, and p lines to 6.5, 4, and 3 G. The measured linewidths in krypton are intermediate to those in argon and xenon.

The substitutional site in an argon lattice is approximately 3.75 Å in diameter. This is also the van der Waals diameter of phosphorus. Since the radical is apparently not rotating, the fluorine atoms may be accommodated in the octahedral holes adjacent to the substitutional site. Using this model of the argon matrix, the environment of each radical would be essentially the same.

When krypton was used as the matrix, the small splittings of ~1 and 5 G in the p and o features indicate that the linewidths may be determined by the environment around the individual radicals and that there may be two preferred sites. Interaction of the radical with the ^{83}Kr nuclei of the matrix would not be expected to give the observed splittings although this may contribute to the linewidth. A molecular model of the krypton matrix and a PF_2 radical indicates that the radical may be accommodated with the fluorine atoms in either the octahedral holes or the tetrahedral holes adjacent to the substitutional site. Use of the tetrahedral holes distorts the lattice slightly when the hard-sphere model is used.

Coupling of the PF_2 radicals with the numerous magnetic nuclei of xenon presumably causes the major line broadening in the xenon matrices. The narrowing of the lines at 50°K probably indicates some motion of the radical relative to the surrounding magnetic nuclei. Since an isotropic spectrum is not observed, the PF_2 radical is not rotating at this temperature. On further warming to 75°K the lines dropped in intensity and disappeared. Line positions remained constant during warm up.

Further evidence for site splitting is observed in the CO_2 matrix. The outer parallel features (a, a', b, and b' in Fig. 8) are clearly doubled. The perpendicular features are more complex than those observed in the rare gas matrices and the extent of the perpendicular spectrum is ~30 G less than that in the rare-gas matrices. Two of the lines in the CO_2 matrix, indicated as r in Fig. 8, decreased in intensity markedly on warming the sample to 60°K. These are considered to be due to unknown radicals, possibly formed by reaction of PF or PF_2 with the matrix. A satisfactory fit with the observed spectrum was found by using the sum of two axial spectra as shown in Fig. 9. The parameters used for this calculation are given in Table IV.

The geometry of the CO_2 lattice shows that PF_2 may only be accommodated in substitutional sites. The two orientations which give the observed spectrum may be caused by the fluorine atoms of the PF_2 radical being in either the tetrahedral holes or the octahedral holes adjacent to the substitutional site.

When the hyperfine tensors for PF_2 in argon and CO_2 matrices are resolved into their isotropic and dipolar parts, these numbers show a remarkable consistency in the dipolar components. The results are given in Table V. The s-type spin density on the phosphorus atom is calculated to change by 0.012 for one of the sites in the perturbing CO_2 matrix. This results in a change in the isotropic hyperfine coupling of a factor of 2. However, the interaction between the nuclei and the p-character of the unpaired electron is found to change less than 5%.

The deviations between the observed and calculated spectra are believed to be due to (1) no correction for the apparent unequal populations in the two sites, (2) underlying extraneous signals from radicals formed by reaction with the matrix, and (3) the variation of line shapes and widths caused by changes of environment around the radicals. The fairly broad error limits indicated in Table IV are our estimates of how much these effects may alter the apparent line positions in the experimental spectra. Because most of the lines are composites of more than one feature, it was not felt that meaningful linewidths could be obtained from the spectra.

ACKNOWLEDGMENTS

We want to thank L. Hodges and V. Dunning for the samples of P_2F_4 and PF_2H, and J. K. Burdett for assistance with the molecular-orbital calculations. Grateful acknowledgement is made to the National Science Foundation for their partial support of this research.